Mechanistic Insights into Oxidative Molecular Layer Deposition of Conjugated Polymers

Quinton K. Wyatt, Katrina G. Brathwaite, Muhammad Ardiansyah, Nikhila C. Paranamana, Kurt R. Brorsen, Matthias J. Young, 1,2,3*

¹Department of Chemistry, University of Missouri, Columbia, Missouri, 65211, United States

²Department of Biomedical, Biological and Chemical Engineering, University of Missouri, Columbia, Missouri, 65211, United States

³Materials Science and Engineering Institute, University of Missouri, Columbia, Missouri, 65211, United States

*Email: matthias.young@missouri.edu

I. Abstract

Oxidative molecular layer deposition (oMLD) promises to enable molecular-level control of polymer structure through monomer-by-monomer growth via sequential, self-limiting, gas-phase surface reactions of monomer(s) and oxidant(s). However, only a few oMLD growth chemistries have been demonstrated to date and limited mechanistic understanding is impairing progress in this field. Here, we examine oMLD growth using ethylenedioxythiophene (EDOT), pyrrole (Py), paraphenylenediamine (PDA), thiophene (Thi), and furan (Fu) monomers. We establish key insights into the surface reaction mechanisms underlying oMLD growth. We specifically identify the importance of a two-electron chemical oxidant with sufficient oxidation strength to oxidize both a surface and a gas-phase monomer to enable oMLD growth. The mechanistic insights we report enable rational molecular assembly of copolymer structures to improve electrochemical capacity. This work is foundational to unlock molecular-level control of redox-active polymer structure and will enable the study of previously intractable questions regarding the molecular origins of polymer properties, allowing us to control and optimize polymer properties for energy storage, water desalination, and sensors.

Introduction

Oxidative molecular layer deposition (oMLD) is a relatively new deposition technique used to form electrically (semi)conductive and redox-active conjugated polymers. oMLD is of growing interest because it provides molecular-level control of conjugated polymer film thickness, yielding uniform thin film polymers that are useful for electrochemical energy conversion and storage, ¹⁻³ sensors^{4,5}, and textiles.⁶⁻⁹ The oMLD technique is a sub-category of molecular layer deposition (MLD), in which complementary bifunctional organic molecules are dosed in alternating exposures to form polymer films, ^{10,11} and is akin to common atomic layer deposition (ALD) processes used to form inorganic films. 12 The oMLD process uses the same monomers and oxidants that are used in conventional solution phase polymerization, but doses these species in the gas phase in sequential chemical exposures, as depicted in Figure 1a. oMLD is distinct from gas phase polymerization studies in which an oxidant and monomer are co-dosed in the gas phase to produce polymer films, ^{13–18} because it separates the gas phase chemical precursors into sequential exposure steps. To date, oMLD processes have been demonstrated using ethylenedioxythiophene (EDOT, Figure 1b)^{8,19,20}, pyrrole (Py, Figure 1c),² paraphenylenediamine (PDA, Figure 1d),² and 3-hexylthiophene (3HT, Figure 1e)⁵ monomers and MoCl₅,⁸ ReCl₅,²⁰ and SbCl₅¹⁹ chemical oxidants. These species undergo self-limiting surface reactions to grow thin-film polymers monomer-by-monomer.

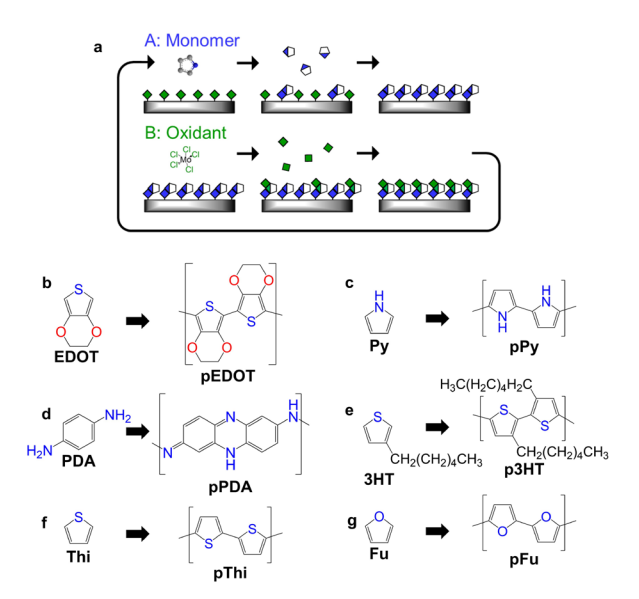


Figure 1. (a) Schematic of oMLD growth proceeding via sequential doses of a monomer and chemical oxidant. Successful oMLD growth has been reported using monomers such as (b) EDOT, (c) Py, (d) PDA, and (e) 3HT. Also shown are (f) thiophene (Thi) and (g) furan (Fu) monomers studied in this work.

Because oMLD proceeds via surface reactions from vapor phase precursors, it does not require the use of side-chains or copolymer additives necessary for solution-based polymer processing. This allows for the formation of chemically pure polymers and enables a fundamental shift in polymer material development (and scientific inquiry), in which polymer properties are dictated by local structure, rather than microstructure or defects. As an example of this, pEDOT coatings formed by oMLD routinely achieve high electrical conductivities of >2000 S/cm^{8,20,21}, and in some reports have achieved conductivities of > 6000 S/cm.¹⁹ In recent work, our group has also expanded beyond oMLD of pEDOT and demonstrated the deposition of pPy by oMLD, achieving record electrochemical capacities of up to 282 mAh/g.² This specific capacity is ~2 times higher than the highest capacities of ~140 mAh/g measured for pPy^{22,23} and is on-par with the electrochemical capacities of next-generation alkali-ion battery materials.^{24,25} The high electrochemical capacity of oMLD pPy (and high electronic conductivity of oMLD pEDOT described above) are attributed to the chemical purity and molecular structure control provided by oMLD growth.

In early studies, the oMLD mechanism has been described as equivalent to homogeneous oxidative polymerization reactions, but spatially constrained to a substrate surface.^{8,20,21} However, recent

work has demonstrated that this picture is incomplete. Some combinations of monomers and oxidants that successfully polymerize in homogenous mixtures do not yield polymers in sequential oMLD doses. For example, EDOT and Br₂ yield pEDOT when mixed homogeneously in vapor or liquid^{26,27}, but do not yield pEDOT films when dosed in sequential pulses.²⁰ Additionally, some reactions do not yield the same products as observed from homogeneous mixtures. For example, primary amines in Ani react to form azo species (e.g. azobenzene) during sequential oMLD doses² instead of forming pAni observed by homogeneous oxidation. Here, we (1) establish key insights into the oMLD growth mechanism that help to explain these unexpected phenomena, (2) identify design rules to guide future development of new oMLD chemistries and processes, and (3) use this understanding to control the molecular assembly of copolymers with record electrochemical capacity.

II. Experimental Section

Oxidative Molecular layer Deposition

Deposition of polymer thin-films by oMLD was carried following previously established conditions.² Briefly, the oMLD reactor chamber was held at 150°C using PID temperature controllers. The reactor chamber operated under a continuous stream of 250 SCCM of ultra-high purity argon carrier gas at reduced pressure (~0.85 Torr). Thiophene (Thi, 98%, Fischer Scientific) and, Furan (Fu, 99%, Fischer Scientific) were held at room temp, while ethylenedioxythiophene (EDOT, 98%, 1PlusChem), paraphenylenediamine (PDA, >97%, Fischer Scientific), and molybdenum pentachloride (MoCl₅, 99.6%, Fischer Scientific) were held at 100 °C, each in a jacketed flow-over precursor bubbler held at a fixed temperature with PID temperature control. All precursors were used as-received and were transferred into the precursor delivery vessels in an argon-filled glovebox. A peak dose pressure of at least ~100 mTorr above base pressure was observed for each monomer precursor dose under these conditions.

The reactor chamber, QCM holder, and sample tray were passivated with the target oMLD chemistry before performing each experiment. Films for ex-situ analysis were deposited on Si wafers (Silicon Valley Microelectronics) and pyrolytic graphite sheets (PGS, Newark). The samples were preheated prior to depositions under inert argon flow for at least 30 min. A typical growth consisted of an A/B dose sequence where the monomer chemical precursor (A) was dosed

for 10 s followed by 100 s of carrier gas purge time, then the MoCl₅ chemical oxidant (B) was dosed for 100 s followed by 100 s of carrier gas purge time. These A/B cycles were repeated to increase the thickness of the resulting polymer films.

Electrochemical Characterization

Polymers deposited onto PGS substrates were characterized by cyclic voltammetry (CV) with a Biologic SP-150 potentiostat using a 3-electrode custom glass electrochemical cell, as described previously.^{2,3} Aqueous electrochemical measurements were performed in 0.1 M NaCl aqueous electrolyte degassed using argon purge at circumneutral pH using an Ag/AgCl reference electrode (BASi) and graphite rod counter electrode (99.999%, Fischer Scientific). CV experiments were performed at a sweep rate of 50 mV/s over a potential range of -1.00 to +1.00 V vs Ag/AgCl, unless otherwise noted.

Raman Spectroscopy

Raman Spectra acquisition was conducted utilizing a Renishaw inVia Raman spectrometer with 633 nm excitation laser. Data was collected over 500–2000 cm⁻¹ with sweeping scan of 10 cm⁻¹/s and a laser power of 10.1 mW.

X-ray photoelectron spectroscopy (XPS)

Select oMLD polymer films were analyzed via XPS using a Thermo Scientific Nexsa instrument with a monochromatic Al Kα X-ray source. These XPS measurements were used to measure incorporation of Fu and Thi into pPy during alternating oMLD exposures. High-resolution scans (200 s acquisition time, 500 ms dwell time, 40 eV pass energy, and 100 meV step size) of O 1s, N 1s and S 2p regions were performed to observe S (Thi) or O (Fu) incorporation into pPy. The peak locations used in this work were charge-corrected to the C 1s peak, centered at an energy of 284.8 eV. The final XPS spectra was analyzed using CasaXPS and plotted using Origin Lab Software.

III. Results and Discussion

To highlight the shortfall of current oMLD mechanistic understanding, we compare *in situ* quartz crystal microbalance (QCM) data acquired during oMLD growth using EDOT vs Thi (Figure 1f)

monomers in Figure 2a. Here, each monomer is dosed in alternating exposures with the MoCl₅ oxidant at 150 °C under ~0.85 Torr (250 sccm) of continuous argon purge in a A:purge:B:purge timing sequence of 10 s: 150 s: 130 s: 150 s. As reported in previous studies, oMLD growth readily proceeds using the EDOT monomer, here exhibiting a mass gain per cycle (MGPC) of ~300 ng/cm²/cycle. But, surprisingly, we do not observe oMLD growth using the Thi monomer (MGPC < 2 ng/cm²/cycle). As shown in the inset of Figure 2a, the Thi monomer represents the core functional structure of EDOT, but without the ethylene-dioxyl substituent. Considering the successful oMLD growth of EDOT:MoCl₅, as well as recent reports of successful oMLD of Py:MoCl₅ and 3HT:MoCl₅,⁵ one would expect that the Thi monomer would undergo oMLD growth, but it does not. This highlights a gap in mechanistic understanding of the oMLD growth mechanism.

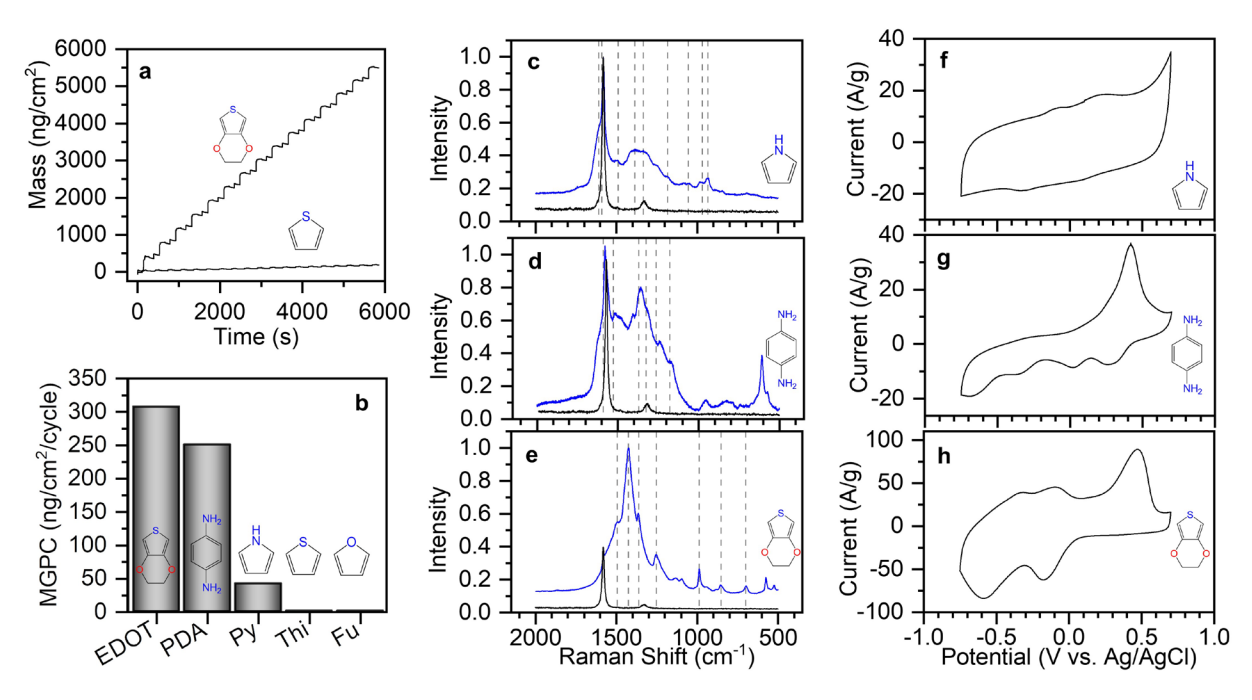


Figure 2. oMLD using EDOT, PDA, Py produced the expected polymers, but surprisingly did not produce polymer films using Thi or Fu monomers. (a) A comparison of EDOT and Thi growth under the same conditions (Dose:Purge, 10s:100s). (b) oMLD steady-state mass gain per cycle (MGPC) of each monomer used with MoCl₅ oxidant. (c-e) Raman spectroscopy of oMLD-formed films (solid blue lines), PGS substrate (solid black lines), and literature references (dashed lines) for (c) pPy^{28–32}, (d) pPDA ³³, (e) pEDOT³⁴. (f-h) Cyclic voltammetry (CV) of oMLD films grown using (f) Py, (g) PDA, (h) EDOT.

In Figure 2b we report the MGPC measured under these same growth conditions for three monomers that have been previously demonstrated by oMLD: EDOT (~300 ng/cm²), PDA (~250 ng/cm²/cycle), and Py (~45 ng/cm²/cycle). We also report the MGPC values measured for Thi and Fu (Figure 1g) monomers in Figure 2b. Fu and Thi do not produce appreciable film growth in QCM experiments. To confirm these results, we also performed depositions on flat samples for ex situ characterization. Spectroscopic ellipsometry (SE) on films deposited on Si witness wafers confirmed the growth behavior in Figure 2b, where EDOT, PDA, and Py exhibited growth rates of ~0.5, 0.98, and 0.3 nm/cycle, respectively, after 100 oMLD cycles, but Fu and Thi produced no detectable films. Raman spectroscopy of the EDOT/MoCl₅ and Py/MoCl₅ oMLD films exhibited characteristic spectra for polypyrrole (pPy), polyparaphenyelenediamine (pPDA) and polyethylenedioxythiophene (pEDOT), respectively (Figure 2c-e), while no Raman response was observed above the background when using Fu and Thi monomers. Likewise, cyclic voltammetry (CV) electrochemical measurements in 0.1 M NaCl electrolyte yielded characteristic electrochemical response consistent with pPy, pPDA, and pEDOT (Figure 2f-h). As reported in recent work, PDA/MoCl₅ produces a blend of phenazine and azo functionality with corresponding mixed redox activity.2 However, we observed no electrochemical response above the bare substrate signal for Fu and Thi monomers. The SE, Raman, and CV data for the samples exposed to Fu/MoCl₅ and Thi/MoCl₅ chemical exposures are reported in the Supporting Information (SI) Section A. Considering the molecular structures of the five monomers studied in Figure 2, there is not a clear pattern as to why Thi and Fu do not exhibit oMLD growth

To understand the failure of oMLD growth using the Fu and Thi monomers, we more carefully examined the QCM data collected during oMLD growth of pEDOT as presented in Figure 3. By examining mass changes during precursor exposures, the mechanistic details of surface reactions can be elucidated.^{35–37} The EDOT monomer was used for these mechanistic studies because polymerization is constrained to the Cα positions due to the ethylene dioxyl ligand, simplifying interpretation. The goal of these QCM studies was to determine the specific monomer and oxidant surface reaction processes and extend this understanding of EDOT reaction mechanisms to understand why Thi and Fu do not react to form polymer films. In Figure 3a we steadily increased the dose times and purge times over the course of the experiment until fully saturating behavior was observed for the EDOT/MoCl₅ growth chemistry. Initial growth conditions reflected previously reported dose/purge times for EDOT (5s/60s) and MoCl₅ (5s/60s), and we observed an

MGPC of ~20 ng/cm² under these conditions. However, recent studies indicate that these dose and purge times may be insufficient for saturation. When increasing dose/purge times from condition (i) to condition (iii) in Figure 3a, we observe an increase in MGPC from 20 ng/cm²/cycle to >300 ng/cm²/cycle. Further increasing the dose and purge times from condition (iv) to condition (v) in Figure 3a did not lead to an increase in MGPC, indicating sufficient dose and purge times at condition (iv). We note that the specific dose and purge times for each precursor are indicated in the inset of Figure 3a. Using condition (iv) from Figure 3a consisting of 10 s EDOT dose, 100 s EDOT purge, 100 s MoCl₅ dose, 100 s MoCl₅ purge, we then examined the mass changes during each precursor dose as depicted in Figure 3b (MoCl₅) and Figure 3c (EDOT) at steady state following > 50 oMLD cycles. We identified a mass gain from the MoCl₅ dose (Δ m₁) of 278 ±5.8 ng/cm² from Figure 3b, and a mass gain from the EDOT dose (Δ m₂) of 71 ±2.7 ng/cm² from Figure 3c. Taking the ratio of Δ m₂/ Δ m₁ to normalize against the number of growth sites yields a value R = 0.26. Using this ratio, R, we can then compare against hypothesized mechanisms to establish a mechanistic picture for EDOT/MoCl₅ oMLD surface reactions.

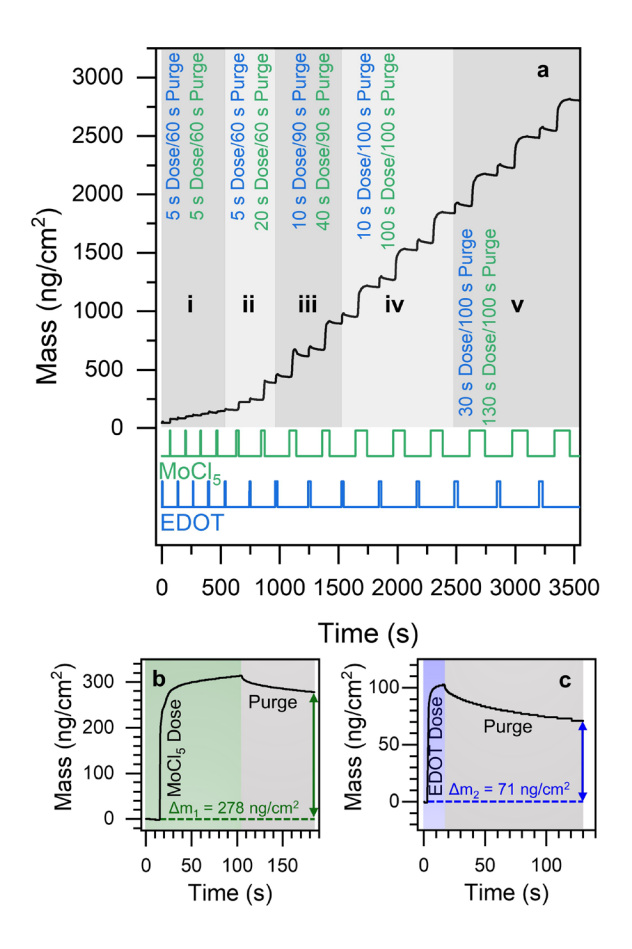


Figure 3. Experimental mass changes during steady-state and saturating oMLD growth of EDOT/MoCl₅ provide mechanistic insights. (a) QCM of oMLD of EDOT/MoCl₅ with increasing dose and purge time of oxidant and monomer until complete saturation is achieved. At steady state, we observe (b) single cycle mass gain for MoCl₅ of ~ 278 ng/cm² and (c) single cycle mass gain for EDOT of ~ 71 ng/cm².

In Figure 4, we propose a reaction mechanism for pEDOT oMLD that is supported by the QCM data collected in Figure 3. In this reaction scheme, MoCl₅ forms a surface adduct with EDOT during the MoCl₅ dose (Figure 4a), and upon subsequent EDOT dose, gas-phase EDOT coordinates to this adduct and MoCl₅ performs a two-electron oxidation via Mo(V)Cl₅ + 2e⁻ → Mo(III)Cl₃ + 2Cl⁻; oxidizing both the surface EDOT monomer and the gas-phase monomer and linking the gas-phase monomer to the surface EDOT (Figure 4b). The net reaction generates 2HCl and MoCl₃, where the MoCl₃ byproduct that remains in the pEDOT film. The theoretical mass gain at each growth site can be calculated from the reaction scheme in Figure 4 by employing tabulated atomic masses of each element to calculate the net mass change on each precursor

exposure. In Figure 4a, one MoCl₅ binds to each active growth site on the surface. The molecular weight (MW) of MoCl₅ is 273.2 g/mol, so we calculate a mass increase of Δm_1 =273.2 g/(mol sites). In Figure 4b, one EDOT molecule (MW=142.2 g/mol) is added and two HCl molecules (MW=36.46 g/mol) are lost per active growth site on the surface, corresponding to a net mass change of Δm_2 =69.28 g/(mol sites). Taking the ratio of $\Delta m_2/\Delta m_1$, we calculate a theoretical mass gain ratio of R=0.2536 for the overall scheme in Figure 4.

This theoretical value of R=0.2536 from Figure 4 is consistent with the experimentally measured value of R=0.26 from Figure 3. We note that in previous reports, the EDOT/MoCl₅ oMLD process is described to proceed via a surface-based polymerization reaction in which the MoCl₅ oxidant reacts with surface EDOT monomers to produce EDOT⁺⁺ + HCl + MoCl₄. In this alternate scheme, one interprets that the HCl and MoCl₄ are inert volatile by-products and the surface EDOT⁺⁺ drives reaction with gas-phase EDOT on the next EDOT exposure. However, this reaction scheme produces a theoretical ratio of R = 2.954 which is not consistent with the value of R=0.26 measured in Figure 3. Furthermore, for surface polymerization to proceed, the gas-phase EDOT must undergo oxidation to form EDOT⁺⁺, and this previously reported mechanistic picture does not explain how this occurs. We also examined other potential reaction schemes and calculated the corresponding R values, and the mechanism we report in Figure 4 is the only mechanism we found that is consistent with our experimental results. For example, coordination of a Mo₂Cl₁₀ dimer to each surface EDOT growth site yields a ratio of R=0.127, only 50% of the measured value. Furthermore, previous reports of a stoichiometric amount of Mo:S in the resulting pEDOT films⁸ are consistent with the mechanism we describe here.

a
$$Cl_{Mo}^{Cl}$$
 Cl_{Cl}^{Cl} Cl_{Cl}^{Cl} Cl_{Cl}^{Cl} Cl_{Cl}^{Cl} Cl_{Cl}^{Cl} Cl_{S}^{Cl} $Cl_{$

Figure 4. Proposed mechanism for oMLD surface reactions during sequential (a) MoCl₅ and (b) EDOT exposures, where (a) MoCl₅ complexes with a surface monomer (Δm_1 =273.2), then (b) during EDOT dose, a surface Mo (IV) species oxidizes both a surface and a gas-phase EDOT monomer and links them together (Δm_2 =69.27), producing nonvolatile MoCl₃ and volatile HCl byproducts. Taking the ratio $\Delta m_2/\Delta m_1$ yields a value of 0.2536 vs. the experimentally measured value of 0.26 from Figure 2.

The reaction scheme in Figure 4 reveals multiple key properties of monomers and oxidants that are necessary for a successful oMLD chemistry. For oMLD growth to proceed, an oxidant must be used which exhibits multiple oxidation states (i.e. Mo, Re, Sb used to date)^{8,20,21} and must undergo two reduction reactions, where both electron uptake processes occur at high enough oxidation potentials to oxidize both a surface monomer and a gas-phase monomer to link them together. In the case of the proposed EDOT oMLD reaction scheme in Figure 4, the oxidant (MoCl₅), oxidizes two EDOT monomers, propagating polymerization by linking the surface EDOT (terminating a pEDOT chain) to the next gas-phase EDOT monomer. One can conceptually separate this into two one-electron oxidation steps for the MoCl₅ oxidant: Mo(V)Cl₅ + e⁻ \rightarrow Mo(IV)Cl₄ + Cl⁻ and Mo(VI)Cl₄ + e⁻ \rightarrow Mo(III)Cl₃ + Cl⁻. These two reactions must together have strong enough oxidation potentials to oxidize both the surface and gas-phase monomers. We propose that this two-electron oxidation process is the underlying reason for the failure of the

oMLD process for the Fu and Thi monomers, where the oxidation power of Mo(IV)Cl₄ is insufficient to oxidize Fu or Thi monomers.

To explore this possibility, we examined the equilibrium redox potentials of the five monomers examined in Figure 2 as well as the equilibrium redox potential of Mo(V)Cl₅/Mo(IV)Cl₄ and Mo(IV)Cl₄/Mo(III)Cl₃. We employed nonaqueous linear sweep voltammetry measurements to measure monomer oxidation potentials as described in SI Section B. We measured onset monomer oxidation potentials of 0.87, 0.74, 1.21, 1.72, and 1.91 V vs. standard hydrogen electrode (SHE) for Py, PDA, EDOT, Thi, and Fu, respectively. We also performed density functional theory (DFT) calculations to determine the oxidation potentials of the Mo(V)Cl₅/Mo(IV)Cl₄ and Mo(IV)Cl₄/Mo(III)Cl₃ redox couples as described in SI Section C. We calculated oxidation potentials of 3.34 and 1.46 V vs. SHE for the Mo(V)Cl₅/Mo(IV)Cl₄ and Mo(IV)Cl₄/Mo(III)Cl₃ redox couples, respectively. A subset of the monomer and oxidant redox potential values have been reported in previous literature and we compare our results against prior reports in SI Sections B and C. An energy diagram of these cumulative results is presented in Figure 5.

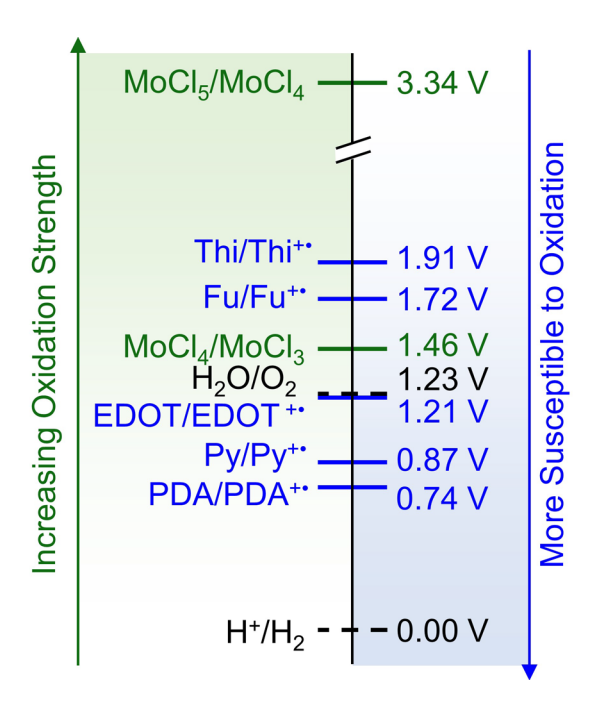


Figure 5. We identify that relative oxidation/reduction potentials can be used as a descriptor to predict the success of a monomer/oxidant combination for an oMLD chemistry. In this schematic depiction, the reduction potentials of oxidants (as calculated by DFT) and monomers (as measured

experimentally) are plotted vs SHE. Oxidants are shown in green and monomers are in blue. Stronger oxidants appear at higher (more positive) potentials and monomers that are more susceptible to oxidation appear at lower (more negative) potentials. The Mo(IV)Cl₄/Mo(III)Cl₃ redox couple does not have sufficient oxidation strength to oxidize Fu or Thi monomers.

In Figure 5, we use the relative oxidation potentials at room temperature from nonaqueous electrochemical measurements and DFT calculations within a vacuum corrected to room temperature as surrogates to identify qualitative trends in the relative oxidation/reduction strength of the monomers and oxidant. Although the oMLD process is carried out at elevated temperature in the gas phase, these reference values provide a conceptual view of the driving forces for oMLD reaction. In Figure 5, the oxidation potentials of Fu and Thi monomers are 1.91 V and 1.72 V vs SHE, respectively³⁹, which are higher than the oxidation power of $Mo(IV)Cl_4 \rightarrow Mo(III)Cl_3$ (1.46 V vs SHE). Although the $Mo(V)Cl_5/Mo(IV)Cl_4$ redox couple is capable of oxidizing one Fu or Thi monomer, the $Mo(IV)Cl_4/Mo(III)Cl_3$ couple has insufficient oxidizing power to oxidize a second monomer and drive surface polymerization, preventing the oMLD reaction from propagating further. Conversely, the oxidation potentials of EDOT, PDA, and Py of 1.21, 0.74 and 0.87 V vs. SHE fall below the oxidation power of $Mo(V)Cl_5 \rightarrow Mo(IV)Cl_4$ and $Mo(IV)Cl_4 \rightarrow Mo(III)Cl_3$, allowing for continued polymer growth of pEDOT, pPDA, and pPy. We also note that oMLD using the 3HT monomer⁵ is viable due to the electron donating hexyl group which lowers the onset potential for oxidation, similar to the ethylene dioxyl group on EDOT.

While the mechanistic insights provided above explain why pure pThi and pFu polymers are inaccessible by oMLD using the MoCl₅ oxidant, this mechanistic picture also suggests that Thi or Fu monomers could be incorporated into pEDOT, pPy or pPDA polymers through controlled molecular assembly. Specifically, if a Py-MoCl₅ adduct is present on the growth surface, based on the conceptual picture in Figure 5, the MoCl₅ oxidant is expected to have enough oxidizing power to oxidize a gas-phase Thi (or Fu) monomer, as well as the surface Py monomer, allowing Thi (or Fu) to link to the surface Py and incorporate into the polymer structure.

To confirm this, we performed oMLD in a two-stage series, alternating between 10 oMLD cycles of the Py/MoCl₅ oMLD chemistry and 10 oMLD cycles using a high oxidation potential monomer (Thi or Fu) for a total of 400 oMLD cycles overall. These depositions can be described by a N[n(t_A:t_{Purge}:t_B:t_{Purge}):m(t_C:t_{Purge}:t_B:t_{Purge})] timing sequence where t_A is the Py dose time, t_B is the MoCl₅ dose time, t_C is the Fu dose time (for pPy:Fu) or Thi dose time (for pPy:Thi), t_{Purge} is the

purge time following each precursor dose, n is the number of A/B oMLD subcycles, m is the number of C/B oMLD subcycles, and N is the number of supercycles. For these depositions, N=20, n=10, t_A=10, t_B=60, t_C=10, and t_{Purge}=60. The pPy:Fu and pPy:Thi molecularly mixed copolymer films had SE thicknesses on Si of 15.4 nm and 17.7 nm, respectively. SE data for these samples is presented in SI Section A. In addition to this SE characterization, the resulting polymer films were analyzed by Raman, XPS, and CV, as described below. We also report data below and in the SI for oMLD pPy films formed at 150°C for comparison, using previously established growth conditions.²

In Figure 6a, we report the Raman spectroscopy data for pure pPy and pPy:Fu and pPy:Thi copolymers. We observe that most of the Raman spectroscopy features for pPy are also present in the pPy:Fu and pPy:Thi molecularly assembled copolymers. These Raman features include the C-C and C=C backbone stretching modes of pPy at 1580-1620 cm⁻¹, the C-C and C-N stretching vibrations at 1490 cm⁻¹, the C-C inter-ring stretching modes at 1386 and 1324 cm⁻¹, and the antisymmetrical C-H in-plane bending vibrations at 1238 cm⁻¹. ^{29,31,32} However we note that in both Figure 6a and 6b, the Raman bipolaron band at 900-1000 cm⁻¹ indicating long-range order in oMLD pPy^{29,30} is attenuated from the addition of Fu and Thi oMLD cycles. The bipolaron molecular unit of pPy is depicted in the inset of Figure 6a for reference. In Figure 6b, we separately plot the Raman bipolaron feature over 880-1020 cm⁻¹ for each of the compositions in Figure 6a. The attenuation of this bipoloran band is consistent with the incorporation of the Fu and Thi monomers into the pPy polymer films, disrupting long-range order in the pPy chains.

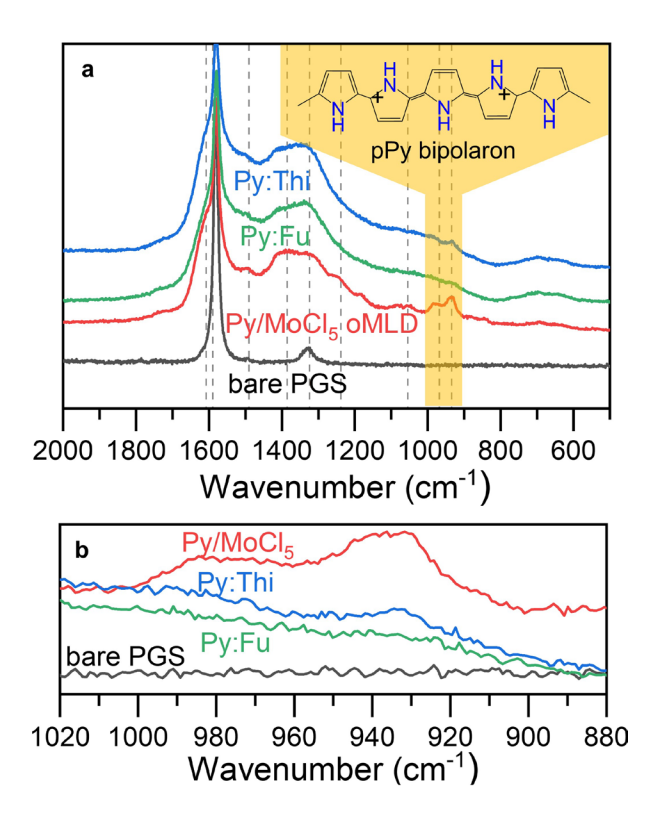


Figure 6. (a) Raman spectroscopy of oMLD pPy as well as pPy:Fu and pPy:Thi formed by alternating 10 cycles of Py and 10 cycles of Fu or Thi oMLD chemistries. The pPy bipolaron bands at 900-1000 cm⁻¹ are highlighted (a) and shown with a zoomed view in (b). The incorporation of Fu and Thi into the pPy structure disrupts the pPy bipolaron band.

Incorporation of Fu and Thi into pPy films was also confirmed using XPS analysis in Figure 7. The XPS elemental compositions of each of the pPy, pPy:Fu, and pPy:Thi samples and discussion are provided in SI Section D. Here, S 2p, N 1s, and O 1s peaks were used to analyze the incorporation of Fu (C₄H₄**O**) and Thi (C₄H₄**S**) monomers into pPy (C₄H₅**N**) polymer films. For the pure pPy oMLD film, we observe no S 1s signature in Figure 7a (as expected), and a clear N 1s peak in Figure 7b consistent with the C₄H₅**N** Py monomer that includes a superposition of C=N⁺, C-N⁺, N-H, and C=N features. In Figure 7c, we observe O 1s peaks at binding energies of 530.7 and 532.4 eV arising from Mo-O and Mo-OH features, respectively, 42,43 due to the reaction of residual MoCl₃ in the oMLD film^{2,8} with air to form MoO_xH_y. For the pPy:Fu copolymer, we observe equivalent XPS signatures for the S 1s and N 1s as observed for pPy. However, distinct from pure oMLD pPy, we observe an increase in the O 1s peak at higher binding energy for the pPy:Fu oMLD film in Figure 7f. The O 1s peak for Fu exhibits a binding energy of 532.2 eV, 44

and we attribute this more pronounced shoulder in Figure 7f to the incorporation of Fu monomers (C₄H₄**O**) into the pPy films. Likewise, we observe a clear peak in the S 2p spectrum for the pPy:Thi copolymer in Figure 7g, indicating the incorporation of the Thi monomer into the pPy:Thi oMLD film. The N 1s and O 1s peaks for the Thi:Py copolymer in Figure 7h and 7i, are consistent the N 1s and O 1s peaks for the pure pPy Figure 7b and 7c. The shoulder in the O 1s peak for the Fu:Py copolymer in Figure 7f and the appearance of S 2p peak for the pPy:Thi copolymer in Figure 7g support the incorporation of Fu and Thi into pPy polymers through alternating chemical exposures. The ability to incorporate Fu and Thi into pPy further validates the mechanistic picture for oMLD described above, where a surface complexed MoCl₅ oxidant is expected to have sufficient oxidation strength to undergo a two-electron oxidation to oxidize and link a surface-bound Py monomer with a gas-phase Fu or Thi monomer.

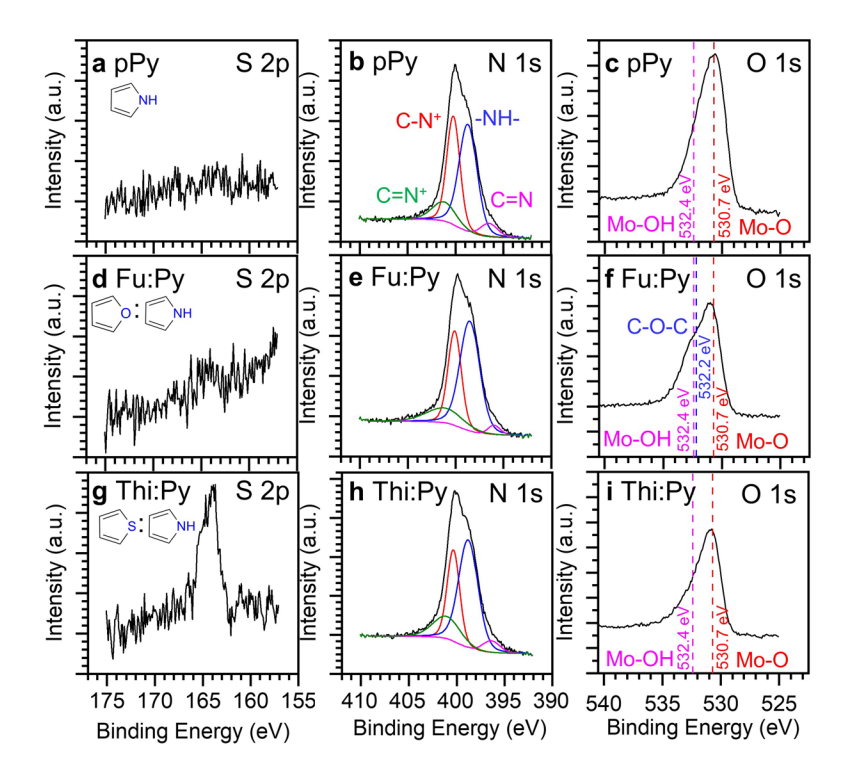


Figure 7. XPS analysis for pPy (a:S 2p, b:N 1s, c:O 1s), pPy:Fu (d:S 2p, e:N 1s, f:O 1s), and pPy:Thi (g:S 2p, h:N 1s, i:O 1s). The additional shoulder at higher binding energy for the O 1s peak confirmed incorporation of Fu into pPy:Fu in (f), while S from Thi was confirmed to incorporate into pPy:Thi in (g).

In Figure 8, we report aqueous CV in 0.1 M NaCl for a 14.3 nm thick oMLD pPy film as well as the pPy:Fu and pPy:Thi copolymers grown using the same scheme described above for the samples examined in Figures 6 and 7. We observe a qualitative shift in the number and location of CV peaks when using only Py monomers (Figure 8a) vs alternating between Py and Fu monomers (Figure 8b) and Py and Thi monomers (Figure 8c). These qualitative differences in the CVs we measure further support that Fu and Thi incorporate into the pPy polymer structure and suggest that the incorporation of these monomers impacts the thermodynamics for electron insertion/extraction into pPy. The addition of Fu monomers to pPy through controlled molecular assembly through oMLD increases the voltage window of electrochemical stability by 0.45 V in Figure 8b, and enhances the redox capacity from 267 mAh/g for pPy to 313 mAh/g for pPy:Fu. Likewise, the addition of Thi monomers to pPy through controlled molecular assembly through oMLD increases the voltage window for electrochemical stability by 0.15 V in Figure 8c, and enhances the redox capacity from 267 mAh/g to 369 mAh/g. By assembling Py and Thi monomers together by oMLD we achieve a 38% enhancement in electrochemical capacity vs. oMLD pPy and achieve 90% of the maximum theoretical charge storage capacity of pPy of 411 mAh/g. ²³ This 369 mAh/g capacity exceeds the highest capacities reported for pPy to date^{2,45,46} and represents a higher capacity than materials currently under consideration for next-generation materials for lithium-ion batteries. ^{24,25}

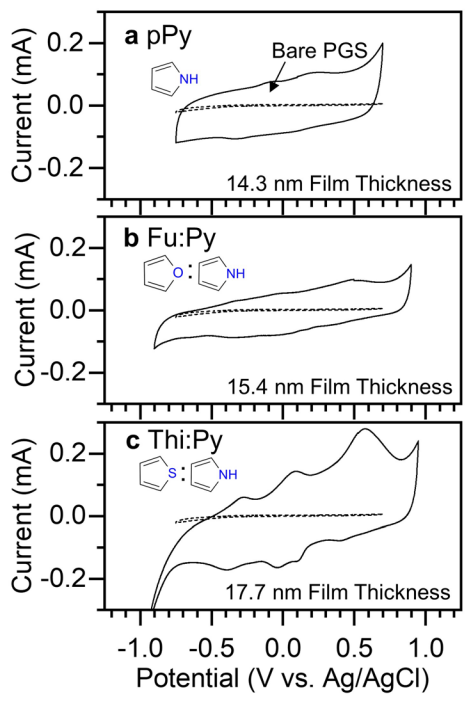


Figure 8. CV of (a) oMLD pPy (b) pPy:Fu, and (c) pPy:Thi films on PGS substrate, measured in 0.1 M NaCl aqueous electrolyte. Incorporating Fu and Thi into the pPy film enhances the electrochemical capacity and potential window for electrochemical activity.

IV. Conclusions

This work establishes a mechanistic picture for the surface reactions responsible for oMLD growth consisting of (1) complexation of a two-electron oxidant to a surface monomer and (2) the oxidation of both a surface and gas-phase monomer by the same oxidant molecule to link the gas-phase monomer to the surface. This mechanistic picture helps explain the success of metal pentachloride two-electron oxidants for oMLD,^{2,8,20,21} and establishes a conceptual picture to guide future exploration of new oMLD growth processes, narrowing the focus to combinations of monomers and oxidants with complimentary oxidation potentials. New two-electron oxidants with higher oxidation strength may enable oMLD of Thi, Fu, and other monomers which are not oxidized as readily as Py, EDOT, PDA, or 3HT. Furthermore, this work suggests that a wide range of monomers with appropriate oxidation potentials^{47,48} could be used with the MoCl₅ oxidant to form polymer films by oMLD. Additionally, the molecular assembly of copolymers of Py with Fu and Thi monomers shown in this work to enhance electrochemical capacity over pure pPy demonstrates a platform for tuning the molecular structure of polymers to access improved

electrochemical properties for applications including energy storage, water desalination, and sensing.

V. Acknowledgements

M.J.Y. acknowledges support from faculty start-up funds provided by the University of Missouri Biomedical, Biological, and Chemical Engineering Department and Department of Chemistry, and M.J.Y. and Q.K.W. acknowledge partial support from the National Science Foundation (NSF) Division of Chemical, Bioengineering, Environmental, & Transport Systems (CBET) through Award Number 2131282. We thank Mahya Mehregan at the University of Missouri for assistance with Raman spectroscopy measurements.

VI. Supporting Information

The following Supporting Information is available free of charge at the ACS website:

A: Additional Characterization of Fu/MoCl5 and Thi/MoCl5 Samples

B: Measurements of Monomer Oxidation Onset Potentials

C: Density Functional Theory (DFT) Calculation Details

VII. References

- (1) Kim, D. H.; Atanasov, S. E.; Lemaire, P.; Lee, K.; Parsons, G. N. Platinum-Free Cathode for Dye-Sensitized Solar Cells Using Poly(3,4-Ethylenedioxythiophene) (PEDOT) Formed via Oxidative Molecular Layer Deposition. ACS Appl Mater Interfaces 2015, 7, 3866–3870. https://doi.org/10.1021/am5084418.
- (2) Wyatt, Q. K.; Vaninger, M.; Paranamana, N. C.; Heitmann, T. W.; Kaiser, H.; Young, M. J. Oxidative Molecular Layer Deposition of Amine-Containing Conjugated Polymer Thin Films. ACS Appl Polym Mater 2022. https://doi.org/10.1021/acsapm.2c00942.
- (3) Wyatt, Q. K.; Young, M. J. Pulsed Electrodeposition of Ultrathin Polyaniline Films and Mechanistic Understanding of Their Anion-Mediated Electrochemical Behavior. *J Electrochem Soc* **2020**, *167*, 110548. https://doi.org/10.1149/1945-7111/aba5d5.

- (4) Ozaydin-Ince, G.; Coclite, A. M.; Gleason, K. K. CVD of Polymeric Thin Films: Applications in Sensors, Biotechnology, Microelectronics/Organic Electronics, Microfluidics, MEMS, Composites and Membranes. *Reports on Progress in Physics* 2012, 75. https://doi.org/10.1088/0034-4885/75/1/016501.
- (5) Tan, H.; Chu, Y.; Wu, X.; Liu, W. J.; Zhang, D. W.; Ding, S. J. High-Performance Flexible Gas Sensors Based on Layer-by-Layer Assembled Polythiophene Thin Films. *Chemistry of Materials* 2021, 33, 7785–7794. https://doi.org/10.1021/ACS.CHEMMATER.1C02182/ASSET/IMAGES/MEDIUM/CM1 C02182 M001.GIF.
- (6) Ding, Y.; Invernale, M. A.; Sotzing, G. A. Conductivity Trends of Pedot-Pss Impregnated Fabric and the Effect of Conductivity on Electrochromic Textile. *ACS Appl Mater Interfaces* **2010**, *2*, 1588–1593. https://doi.org/10.1021/AM100036N.
- (7) Laforgue, A. All-Textile Flexible Supercapacitors Using Electrospun Poly(3,4-Ethylenedioxythiophene) Nanofibers. *J Power Sources* **2011**, *196*, 559–564. https://doi.org/10.1016/J.JPOWSOUR.2010.07.007.
- (8) Atanasov, S. E.; Losego, M. D.; Gong, B.; Sachet, E.; Maria, J. P.; Williams, P. S.; Parsons, G. N. Highly Conductive and Conformal Poly(3,4-Ethylenedioxythiophene) (PEDOT) Thin Films via Oxidative Molecular Layer Deposition. *Chemistry of Materials* 2014, 26, 3471–3478. https://doi.org/10.1021/cm500825b.
- (9) Brozena, A. H.; Oldham, C. J.; Parsons, G. N. Atomic Layer Deposition on Polymer Fibers and Fabrics for Multifunctional and Electronic Textiles. *Journal of Vacuum Science* & Technology A: Vacuum, Surfaces, and Films 2016, 34, 010801. https://doi.org/10.1116/1.4938104.
- (10) George, S. M.; Dameron, A. A.; Yoon, B. Surface Chemistry for Molecular Layer Deposition of Organic and Hybrid Organic-Inorganic Polymers. *Acc Chem Res* 2009, 42, 498–508. https://doi.org/10.1021/AR800105Q.

- (11) Yoshimura, T.; Tatsuura, S.; Sotoyama, W. Polymer Films Formed with Monolayer Growth Steps by Molecular Layer Deposition. *Appl Phys Lett* **1991**, *59*, 482–484. https://doi.org/10.1063/1.105415.
- (12) George, S. M. Atomic Layer Deposition: An Overview. *Chem Rev* **2010**, *110*, 111–131. https://doi.org/10.1021/CR900056B.
- (13) Smolin, Y. Y.; Soroush, M.; Lau, K. K. S. Oxidative Chemical Vapor Deposition of Polyaniline Thin Films. *Beilstein Journal of Nanotechnology* **2017**, *8*, 1266–1276. https://doi.org/10.3762/bjnano.8.128.
- (14) Lock, J. P.; Lutkenhaus, J. L.; Zacharia, N. S.; Im, S. G.; Hammond, P. T.; Gleason, K. K. Electrochemical Investigation of PEDOT Films Deposited via CVD for Electrochromic Applications. *Synth Met* 2007, *157*, 894–898. https://doi.org/10.1016/j.synthmet.2007.08.022.
- (15) Wang, X.; Zhang, X.; Sun, L.; Lee, D.; Lee, S.; Wang, M.; Zhao, J.; Shao-Horn, Y.; Dincă, M.; Palacios, T.; Gleason, K. K. High Electrical Conductivity and Carrier Mobility in OCVD PEDOT Thin Films by Engineered Crystallization and Acid Treatment. *Sci Adv* 2018, 4, 1–10. https://doi.org/10.1126/sciadv.aat5780.
- (16) Smolin, Y. Y.; Soroush, M.; Lau, K. K. S. Influence of OCVD Polyaniline Film Chemistry in Carbon-Based Supercapacitors. *Ind Eng Chem Res* **2017**, *56*, 6221–6228. https://doi.org/10.1021/acs.iecr.7b00441.
- (17) Im, S. G.; Gleason, K. K. Systematic Control of the Electrical Conductivity of Poly(3,4-Ethylenedioxythiophene) via Oxidative Chemical Vapor Deposition. *Macromolecules* 2007, 40, 6552–6556. https://doi.org/10.1021/ma0628477.
- (18) Bilger, D.; Homayounfar, S. Z.; Andrew, T. L. A Critical Review of Reactive Vapor Deposition for Conjugated Polymer Synthesis. *J Mater Chem C Mater* **2019**, *7*, 7159–7174. https://doi.org/10.1039/c9tc01388a.
- (19) Volk, A. A.; Kim, J.-S.; Jamir, J.; Dickey, E. C.; Parsons, G. N. Oxidative Molecular Layer Deposition of PEDOT Using Volatile Antimony(V) Chloride Oxidant.

- Journal of Vacuum Science & Technology A: Vacuum, Surfaces, and Films 2021, 39, 032413. https://doi.org/10.1116/6.0000791.
- (20) Ghafourisaleh, S.; Popov, G.; Leskelä, M.; Putkonen, M.; Ritala, M. Oxidative MLD of Conductive PEDOT Thin Films with EDOT and ReCl5as Precursors. *ACS Omega* 2021, 6, 17545–17554. https://doi.org/10.1021/acsomega.1c02029.
- (21) Volk, A. A.; Kim, J.-S.; Jamir, J.; Dickey, E. C.; Parsons, G. N. Oxidative Molecular Layer Deposition of PEDOT Using Volatile Antimony(V) Chloride Oxidant. *Journal of Vacuum Science & Technology A* **2021**, *39*, 032413. https://doi.org/10.1116/6.0000791.
- (22) Rajagopalan, B.; Kim, B.; Hur, S. H.; Yoo, I. K.; Chung, J. S. Redox Synthesis of Poly (p–Phenylenediamine)–Reduced Graphene Oxide for the Improvement of Electrochemical Performance of Lithium Titanate in Lithium–Ion Battery Anode. *J Alloys Compd* **2017**, 709, 248–259. https://doi.org/10.1016/J.JALLCOM.2017.03.166.
- (23) Fong, K. D.; Wang, T.; Smoukov, S. K. Multidimensional Performance Optimization of Conducting Polymer-Based Supercapacitor Electrodes. *Sustain Energy Fuels* **2017**, *1*, 1857–1874. https://doi.org/10.1039/c7se00339k.
- (24) Tian, Y.; Zeng, G.; Rutt, A.; Shi, T.; Kim, H.; Wang, J.; Koettgen, J.; Sun, Y.; Ouyang, B.; Chen, T.; Lun, Z.; Rong, Z.; Persson, K.; Ceder, G. Promises and Challenges of Next-Generation "beyond Li-Ion" Batteries for Electric Vehicles and Grid Decarbonization.

 Chem Rev 2021, 121, 1623–1669. https://doi.org/10.1021/acs.chemrev.0c00767.
- (25) Whittingham, M. S. Special Editorial Perspective: Beyond Li-Ion Battery Chemistry. *Chem Rev* **2020**, *120*, 6328–6330. https://doi.org/10.1021/acs.chemrev.0c00438.
- (26) Chelawat, H.; Vaddiraju, S.; Gleason, K. Conformal, Conducting Poly(3,4-Ethylenedioxythiophene) Thin Films Deposited Using Bromine as the Oxidant in a Completely Dry Oxidative Chemical Vapor Deposition Process. *Chemistry of Materials* 2010, 22, 2864–2868. https://doi.org/10.1021/cm100092c.
- (27) Patra, A.; Agrawal, V.; Bhargav, R.; Shahjad; Bhardwaj, D.; Chand, S.; Sheynin, Y.; Bendikov, M. Metal Free Conducting PEDOS, PEDOT, and Their Analogues via an

- Unusual Bromine-Catalyzed Polymerization. *Macromolecules* **2015**, *48*, 8760–8764. https://doi.org/10.1021/acs.macromol.5b01777.
- (28) Liu, Y. C.; Hwang, B. J. Identification of Oxidized Polypyrrole on Raman Spectrum. *Synth Met* **2000**, *113*, 203–207. https://doi.org/10.1016/S0379-6779(00)00188-0.
- (29) Trchová, M.; Stejskal, J. Resonance Raman Spectroscopy of Conducting Polypyrrole Nanotubes: Disordered Surface versus Ordered Body. *Journal of Physical Chemistry A* 2018, 122, 9298–9306. https://doi.org/10.1021/acs.jpca.8b09794.
- (30) Santos, M. J. L.; Brolo, A. G.; Girotto, E. M. Study of Polaron and Bipolaron States in Polypyrrole by in Situ Raman Spectroelectrochemistry. *Electrochim Acta* **2007**, *52*, 6141–6145. https://doi.org/10.1016/j.electacta.2007.03.070.
- (31) Gupta, S. Hydrogen Bubble-Assisted Syntheses of Polypyrrole Micro/Nanostructures Using Electrochemistry: Structural and Physical Property Characterization. *Journal of Raman Spectroscopy* **2008**, *39*, 1343–1355. https://doi.org/10.1002/jrs.2002.
- (32) Furukawa, Y.; Tazawa, S.; Fujii, Y.; Harada, I. Raman Spectra of Polypyrrole and Its 2,5-13C-Substituted and C-Deuterated Analogues in Doped and Undoped States. *Synth Met* 1988, 24, 329–341. https://doi.org/10.1016/0379-6779(88)90309-8.
- (33) do Nascimento, G. M.; Sestrem, R. H.; Temperini, M. L. A. Structural Characterization of Poly-Para-Phenylenediamine-Montmorillonite Clay Nanocomposites. *Synth Met* 2010, 160, 2397–2403. https://doi.org/10.1016/j.synthmet.2010.09.016.
- (34) Chang, S. H.; Chiang, C. H.; Kao, F. S.; Tien, C. L.; Wu, C. G. Unraveling the Enhanced Electrical Conductivity of PEDOT:PSS Thin Films for ITO-Free Organic Photovoltaics. *IEEE Photonics J* **2014**, *6*. https://doi.org/10.1109/JPHOT.2014.2331254.
- (35) Lee, Y.; Sun, H.; Young, M. J.; George, S. M. Atomic Layer Deposition of Metal Fluorides Using HF-Pyridine as the Fluorine Precursor. *Chemistry of Materials* **2016**, *28*, 2022–2032. https://doi.org/10.1021/acs.chemmater.5b04360.

- (36) Elam, J. W.; Groner, M. D.; George, S. M. Viscous Flow Reactor with Quartz Crystal Microbalance for Thin Film Growth by Atomic Layer Deposition. *Review of Scientific Instruments* **2002**, *73*, 2981–2987. https://doi.org/10.1063/1.1490410.
- (37) Puurunen, R. L. Surface Chemistry of Atomic Layer Deposition: A Case Study for the Trimethylaluminum/Water Process. *J Appl Phys* **2005**, *97*, 1–52. https://doi.org/10.1063/1.1940727.
- (38) Jain, H.; Poodt, P. About the Importance of Purge Time in Molecular Layer Deposition of Alucone Films. *Dalton Transactions* 2021, 50, 5807–5818. https://doi.org/10.1039/d1dt00623a.
- (39) Weinberg, N. L.; Weinberg, H. R. Electrochemical Oxidation of Organic Compounds. Chem Rev 1968, 68, 449–523. https://doi.org/10.1021/CR60254A003/ASSET/CR60254A003.FP.PNG_V03.
- (40) Tabačiarová, J.; Mičušík, M.; Fedorko, P.; Omastová, M. Study of Polypyrrole Aging by XPS, FTIR and Conductivity Measurements. *Polym Degrad Stab* **2015**, *120*, 392–401. https://doi.org/10.1016/j.polymdegradstab.2015.07.021.
- (41) Atanasoska, L.; Naoi, K.; Smyrl, W. H. XPS Studies On Conducting Polymers: Polypyrrole Films Doped With Perchlorate And Polymeric Anions. *Chemistry of Materials* **1992**, *4*, 988–994. https://doi.org/10.1021/cm00023a012.
- (42) Guimond, S.; Göbke, D.; Sturm, J. M.; Romanyshyn, Y.; Kuhlenbeck, H.; Cavalleri, M.; Freund, H. J. Well-Ordered Molybdenum Oxide Layers on Au(111): Preparation and Properties. *Journal of Physical Chemistry C* 2013, 117, 8746–8757. https://doi.org/10.1021/jp3113792.
- (43) Mane, A. A.; Moholkar, A. v. Orthorhombic MoO 3 Nanobelts Based NO 2 Gas Sensor. *Appl Surf Sci* **2017**, *405*, 427–440. https://doi.org/10.1016/j.apsusc.2017.02.055.
- (44) Qiao, M. H.; Tao, F.; Cao, Y.; Li, Z. H.; Dai, W. L.; Deng, J. F.; Xu, G. Q. Cycloaddition Reaction of Furan with Si(100)-2×1. *Journal of Chemical Physics* **2001**, *114*, 2766–2774. https://doi.org/10.1063/1.1338477.

- (45) Fan, L. Z.; Maier, J. High-Performance Polypyrrole Electrode Materials for Redox Supercapacitors. *Electrochem commun* **2006**, *8*, 937–940. https://doi.org/10.1016/j.elecom.2006.03.035.
- (46) Khomenko, V.; Frackowiak, E. Determination of the Specific Capacitance of Conducting Polymer / Nanotubes Composite Electrodes Using Different Cell Configurations. **2005**, *50*, 2499–2506. https://doi.org/10.1016/j.electacta.2004.10.078.
- (47) Weinberg, N. L.; Weinberg, H. R. Electrochemical Oxidation of Organic Compounds. *Chem Rev* **1968**, *68*, 449–523. https://doi.org/10.1021/cr60254a003.
- (48) Roth, H. G.; Romero, N. A.; Nicewicz, D. A. Experimental and Calculated Electrochemical Potentials of Common Organic Molecules for Applications to Single-Electron Redox Chemistry. *Synlett* 2016, 27, 714–723. https://doi.org/10.1055/s-0035-1561297.

For Table of Contents Only:

